PHYSICAL REVIEW B **95**, 174519 (2017)

High-pressure behavior of superconducting boron-doped diamond

Mahmoud Abdel-Hafiez,[1] Dinesh Kumar,[2] R. Thiyagarajan,[3] Q. Zhang,[3] R. T. Howie,[3] K. Sethupathi,[4] O. Volkova,[5,6,7] A. Vasiliev,[5,7,8] W. Yang,[3] H. K. Mao,[3] and M. S. Ramachandra Rao[2]

[1]*Center for High Pressure Science and Technology Advanced Research, Beijing 100094, China*

[2]*Department of Physics, Nano Functional Materials Technology Centre and Materials Science Research Centre, Indian Institute of Technology Madras, Chennai 600036, Tamil Nadu, India*

[3]*Center for High Pressure Science and Technology Advanced Research, Shanghai 201203, China*

[4]*Department of Physics, Low Temperature Physics Laboratory, Indian Institute of Technology (IIT) Madras, Chennai 600036, Tamil Nadu, India*

[5]*Low Temperature Physics and Superconductivity Department, Physics Faculty, M. V. Lomonosov Moscow State University, Moscow 119991, Russia*

[6]*Theoretical Physics and Applied Mathematics Department, Ural Federal University, Ekaterinburg 620002, Russia*

[7]*National University of Science and Technology "MISiS", Moscow 119049, Russia*

[8]*National Research South Ural State University, 454080 Chelyabinsk, Russia*

(Received 6 March 2017; revised manuscript received 4 May 2017; published 25 May 2017)

This work investigates the high-pressure structure of freestanding superconducting ($T_c = 4.3$ K) boron-doped diamond (BDD) and how it affects the electronic and vibrational properties using Raman spectroscopy and x-ray diffraction in the 0–30 GPa range. High-pressure Raman scattering experiments revealed an abrupt change in the linear pressure coefficients, and the grain boundary components undergo an irreversible phase change at 14 GPa. We show that the blueshift in the pressure-dependent vibrational modes correlates with the negative pressure coefficient of T_c in BDD. The analysis of x-ray diffraction data determines the equation of state of the BDD film, revealing a high bulk modulus of $B_0 = 510 \pm 28$ GPa. The comparative analysis of high-pressure data clarified that the sp^2 carbons in the grain boundaries transform into hexagonal diamond.

DOI: 10.1103/PhysRevB.95.174519

I. INTRODUCTION

Diamond exhibits complex electronic transformations as the boron concentration is raised high enough to drive an otherwise insulating system to a metallic regime. It is here that merging of the impurity and valence bands results in superconductivity in diamond [1]. Over a decade of research has shown a steady improvement in the diamond superconducting transition temperature T_c, from an initial report [2] of 2.3 K to 10 K, as reported in the most recent work [3]. More interestingly, Moussa *et al.* report that the T_c in diamond can be raised up to 55 K with efficient doping [4]. However, for all practical purposes, beyond a certain boron concentration ($>10^{19}$ cm^{-3}) the formation of a multiboron complex, the segregation of boron, vacancies, and interstitial boron have impeded an increase in the active carrier concentration required to achieve the above predicted T_c [5]. In fact, in polycrystalline boron-doped diamond (BDD), it is estimated that only 10% of the incorporated boron atoms are isolated substitutional boron atoms, whereas the remaining boron atoms are either consumed by the grain boundaries or become point defects that are inactive or even detrimental to the T_c [6,7].

Despite great efforts in the study of group-IV covalent semiconductors, many unresolved questions and unexplained results require further investigation. These include establishing the nature of their superconducting coupling mechanism [7–11]. The discovery of superconductivity in diamond was immediately followed by theoretical works from various groups stressing the study of the mechanism of superconductivity in BDD. *Ab initio* calculations [9,10] have revealed that beyond the critical concentration $n_c = 4.5 \times 10^{20}$ cm^{-3} [12], an insulator-to-metal transition (IMT) sets in and the impurity band merges with the valence band, driving the Fermi level into the valence band. For such degenerate semiconductors, it becomes energetically favorable for Cooper pair formation via the coupling of holes with a zone center phonon (ZCP). If $\lambda_{\text{el-ph}}$ is the electron-phonon coupling constant and ω is the ZCP frequency, then BCS theory estimates the superconducting transition temperature T_c, using $T_c \sim \omega \exp(\frac{-1}{\lambda_{\text{el-ph}}})$. Contrary to the phonon-mediated pairing mechanism, an alternative theory proposed by Baskaran suggests the existence of a rigid impurity band in the valence band of superconducting BDD, where the width of the impurity band provides an estimate of T_c [11,13]. The present experimental results appear to favor the BCS mechanism, and this finding will be emphasized later in the paper. In addition, several questions can be raised; in particular, does granular superconducting BDD undergo a phase change at high pressure? How compressible is superconducting diamond? More generally, high-pressure investigations in pure diamond have undoubtedly established that cubic diamond is highly incompressible and it retains its cubic structure even up to 140 GPa [14]. On the other hand, graphite undergoes a phase transformation at 14 GPa [15]. This is because the covalently bonded hexagonal planes in graphite are connected by weak van der Waals bonds that can be easily deformed. Owing to puckering of its hexagonal planes, sp^2-hybridized carbon atoms transform into sp^3-hybridized carbon atoms. The general consensus is that graphite transforms into lonsdaleite at 14 GPa, also known as hexagonal diamond, with relatively large lattice parameters of $a = 2.52$ Å and $c = 4.12$ Å compared to $a = 1.54$ Å, for its cubic counterpart [15–17]. As granular BDD consists of both sp^2- and sp^3-hybridized networks, it can be regarded

as an ideal system to manifest the above-mentioned changes under high pressure. Most of the work after the discovery of superconductivity in BDD is based on the more relevant sp^3 networks in the grains, and therefore the present state of knowledge on how boron atoms are accommodated in the sp^2 matrix is vague [7,18–23]. Finding a phase change in the heavily doped sp^2- and sp^3-hybridized networks at high pressures would solve a longstanding mystery.

To answer these intriguing questions about the phase change and compressibility of granular superconducting BDD, and also to shed light on the origin of its superconductivity, we deposited a freestanding 60 μm thick BDD film using the hot filament chemical deposition (HFCVD) technique. This method can achieve a high T_c with sufficient grain boundary content that could reveal phase changes at high pressure and also provide an opportunity to explore the relevance of phonon-mediated mechanisms in BDD.

II. EXPERIMENTAL DETAILS

BDD film was grown using the hot filament chemical vapor deposition (HFCVD) technique. Prior to deposition, the silicon substrate was seeded with a commercially obtained nanodiamond solution immersed in a dimethyl sulfoxide solution. After loading the pretreated substrate, the chamber was evacuated to a base pressure of 10^{-3} Torr. The filaments were heated to 2200 °C by passing a high current across its ends. A Si substrate was placed at a suitable distance away from the filaments such that the temperature around it was 850 °C. Deposition was carried out by maintaining the chamber pressure at 7 Torr. CH_4, H_2, and $(CH_3)_3B$ flow rates were maintained at 80, 3000, and 35 sccm, respectively. Further details on the HFCVD reactor can be found elsewhere [24]. After deposition for 110 h, the Si substrate was etched away using a KOH solution, leaving behind a freestanding 60 μm thick BDD film with grain sizes < 1 μm. The surface morphology and the thickness of the BDD sample were determined using scanning electron microscopy (SEM) [Quanta three-dimensional (3D) field emission gun (FEG) microscope].

Electrical transport, specific heat measurements, and magnetic measurements were carried out using a physical property measurement system (PPMS). Resistance measurements down to 100 mK were performed using a dilution refrigerator. Four contacts were used to measure the high-pressure resistivity. A hydrostatic pressure up to 30 GPa was generated using a symmetrical diamond anvil cell device (DAC) employing diamond anvils with a culet size of 300 μm with silicon oil as a pressure medium. A sample of size 50 μm was placed in a 150 μm diam hole on a stainless steel (SS) T301 gasket. The laser wavelength used for the Raman measurement was 632.8 nm He-Ne laser using gratings of 1800 gr/mm. High-pressure Raman spectra were carried out at HPSTAR, China. The *in situ* high-pressure x-ray diffraction experiments were carried out using the synchrotron facility at the High-Pressure Collaborative Access Team (HPCAT) at the Advanced Phonon Source (APS), USA, with a wavelength of 0.3100 Å. The diffraction data were recorded with two-dimensional (2D) images, then DIOPTAS was used for integration, and the structure was refined to analyze the x-ray diffraction (XRD) data. For the *in situ* high-pressure studies, the pressures were determined by the ruby fluorescence method. Ruby chips were put near the crystal and NaCl powders were dropped, surrounding the crystal to serve as pressure transmitting medium. The pressure was monitored by ruby fluorescence [25].

III. RESULTS AND DISCUSSIONS

A. Thermodynamic measurements

We ascertained the bulk superconductivity of a 60 μm thick granular superconducting BDD film using electrical transport, magnetic, and specific heat studies. The resistivity versus temperature curve of the thick BDD film presented in Fig. 1(a) shows the sample's weak semiconducting behavior at higher temperatures, followed by a sharp drop in resistivity with an offset superconducting transition at $T_c = 4.3$ K. This can also be seen by the diamagnetic response of the BDD film in Fig. 1(d).

The critical temperature dependencies of H_{c2} were extracted using the 90% ρ_n criteria from the magnetoresistance curves to 100 mK. Here, ρ_n represents the resistivity just above the onset T_c. Unlike in the case of single crystalline superconducting BDD [26], a Ginzburg-Landau (GL) extrapolation, as represented by the blue curve, does not reproduce the data at low temperatures. Hence, we adopted the Werthamer-Helfand-Hohenberg (WHH) model [the olive-colored curve in Fig. 1(c)] to fit the $H_{c2}(T)$ vs T_c plot. The WHH theory predicts the behavior of $H_{c2}(T)$ in the dirty limit taking into account paramagnetic and orbital pair breaking [27]. The temperature dependence of H_{c2} is given by the WHH formula

$$\ln\frac{1}{t} = \sum_{\nu=-\infty}^{\infty}\left\{\frac{1}{2\nu+1} - \left[2\nu+1+\frac{\bar{h}}{t}+\frac{\left(\frac{\alpha\bar{h}}{t}\right)^2}{2\nu+1+\frac{\bar{h}+\lambda_{so}}{t}}\right]^{-1}\right\}, \quad (1)$$

where $t = \frac{T}{T_c}$, $\bar{h} = \frac{4}{\pi^2}H_{c2}(T)|\frac{dH_{c2}}{dT}|^{-1}_{T_c}$, α is the Maki parameter which describes the relative strength of orbital breaking and the limit of paramagnetism, and λ_{so} is the spin-orbit scattering constant. The orbital limited upper critical field H_{c2} at zero temperature is determined by the slope at T_c as $H_{c2} = 0.69T_c\frac{\partial H_{c2}}{\partial T}|_{T_c}$. The curve of $H_{c2}(T)$ had a slope $-\frac{dH_{c2}}{dT} = 2.19$ T/K for 90% ρ_n. Thus, a fit to the data in the whole measurement range for negligible spin-paramagnetic effects ($\alpha = 0$) and spin-orbit scattering ($\lambda = 0$) yields $\mu_0 H_{c2} = 5.9$ T [27–29]. The coherence length was estimated using $\xi_{GL} = (\frac{\phi_0}{2\pi H_{c2}^{WHH}(0)})^{\frac{1}{2}} = 7.4$ nm, where ϕ_0 is the flux quantum. This is in close agreement with $\xi_{GL} = 7.1$ and 10 nm, as found by Zhang *et al.* [22] and Ekimov *et al.* [2], respectively. While superconductivity is well distinguished by resistivity and magnetization measurements, we further confirmed the bulk superconductivity by performing low-temperature heat capacity measurements down to 0.4 K, as illustrated in Fig. 1(d). Specific heat has probably the best energy resolution among all experimental probes for distinguishing the bulk superconductivity [33–36]. Sidorov *et al.* conducted specific heat measurements on high-pressure high-temperature (HPHT) grown BDD, revealing the existence of enormous inhomogeneity

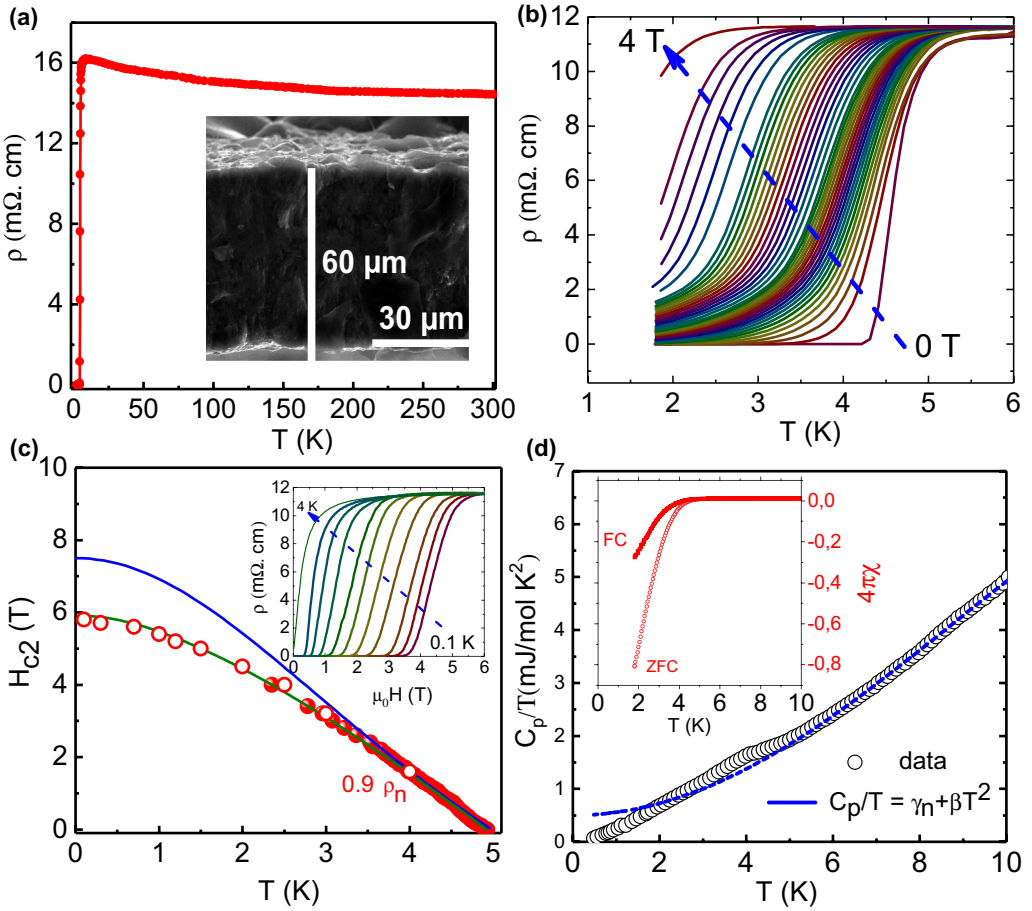

FIG. 1. (a) Resistivity vs temperature curve for the BDD film with a boron concentration $n_B = 2.7 \times 10^{21}$ cm^{-3}, as estimated using Raman spectroscopy [30–32]. Inset: Cross-sectional SEM image of the 60 μm thick BDD film. (b) and the inset of (c) present the temperature and field dependence down to 100 mK of transport measurements of 60 μm thick BDD film. (c) illustrates the upper critical field H_{c2} extracted using the 90% ρ_n criteria. Open symbols are taken from the resistivity vs magnetic field curves. (d) Temperature dependence of the total specific heat in zero magnetic field. The solid line is the specific heat fitting below 10 K using $C_p/T = \gamma_n + \beta T^2$; here, the inset illustrates the temperature dependence of the magnetic susceptibility χ, in an external field of 10 Oe. χ was deduced from the dc magnetization, measured by following the zero-field-cooled (ZFC) and field-cooled (FC) protocols.

in their sample [37]. We performed measurements on a CVD-grown superconducting BDD, which is known to be macroscopically homogeneous [38]. Low-temperature specific heat data are plotted as C_p/T vs T in Fig. 1(d). We observed a clear anomaly at $T_c = 4.8$ K, close to that determined by our resistivity and magnetization measurements. The zero-field specific heat above T_c were well fitted to $C_p/T = \gamma_n + \beta T^2$, with γ_n and β the electronic and lattice coefficients, respectively [as indicated by the dashed line in Fig. 1(d)]. We found $\gamma_n = 0.5$ mJ/mol K^2 and the Debye temperature was extracted using the relation $\theta_D = (12\pi^4 RN/5\beta)^{1/3}$. We obtained $\theta_D = 1410(5)$ K, which is comparable to the value ($\theta_D = 1440$ K) reported by Sidorov *et al.* Clearly, this is less than θ_D (=1880 K) [39] for the single crystalline diamond, a result of lattice softening to due heavy boron doping.

B. High-pressure Raman

We first discuss our Raman spectroscopy data which suggest a possible phase change at 14 GPa. The Raman spectrum recorded at ambient pressure and the decompressed spectrum are presented in Fig. 2(a). The broad peak at 455 cm^{-1} is due to the B-B dimer, an A_{1g} stretching mode. The peaks at 1000 and 1204 cm^{-1} are due to the phonon density of states [9,40]. The hump at 1280 cm^{-1} is due to the Fano resonance of the ZCP of diamond. The graphitic components have Raman signals in higher wave numbers (1350–1550 cm^{-1}) [23,30,41–43]. We have omitted the Raman modes around 1300 cm^{-1} because strong signals from the diamond anvil masked the signals from BDD. Systematic changes of the BDD Raman bands under hydrostatic pressure up to 23 GPa are presented in Fig. 2(b) and the corresponding changes are shown in Fig. 2(c). The values of the pressure coefficients for various Raman modes are listed in Table I. All the peaks in the Raman spectra clearly undergo a blueshift with a hydrostatic pressure increase and the pressure coefficient of the B-B mode was the highest. The higher-frequency vibrational modes related to the grain boundaries disintegrated and vanished completely at pressures close to 14 GPa. The pressure coefficient for all the modes that were available up to 23 GPa doubled abruptly at 14 GPa.

The blueshift in the Raman modes is due to the frequency dependence of its force constants [44]. Additionally, in BDD, the B-B bond length (1.94 Å) is larger than the C-C bond

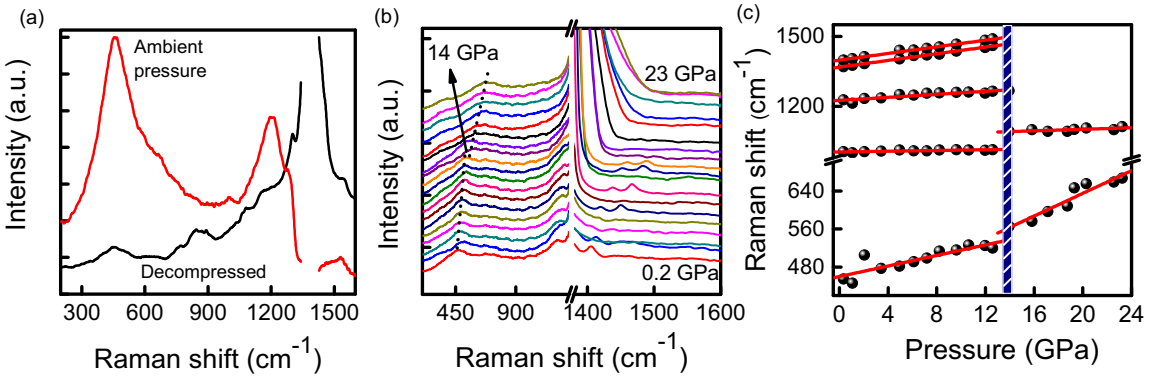

FIG. 2. (a) Raman spectra of BDD at ambient pressure (red) and the decompressed Raman spectrum at 0.2 GPa (black). (b) Raman spectra of freestanding BDD under hydrostatic pressure; dotted lines indicate the abrupt change in the pressure coefficient at 14 GPa. The intense signal at $\sim$1300 cm^{-1} is due to the diamond anvil. (c) Pressure dependence of various vibrational modes in the superconducting BDD; solid spheres represent the peak center obtained using a Gaussian fit on various peaks and the solid line represents a linear fit. Here, the hatched line indicates an abrupt change in the pressure coefficient.

length (1.54 Å). This directly infers that B-B bond compression is much easier compared to C-C bond compression, and thus the pressure coefficient of the B-B mode is relatively high. Close examination of the Raman spectra in the higher-frequency region shows various Raman modes originating from the grain boundaries, including the Raman signals at 1370 cm^{-1} (D peak), 1450 cm^{-1} (*trans*-polyacetylene), and the graphitic 1550 cm^{-1} peak. In our experiment, the Raman bands around 1370 and 1550 cm^{-1} vanished completely above 14 GPa, suggesting a phase change of the grain boundary sp^2 complex. The sp^2 components can be buckled or puckered, thereby facilitating a quicker phase change under compression. Such a phase change is a well-known phenomenon in *trans*-polyacetylene and graphite, where they undergo an irreversible phase change into hexagonal diamond at pressures above 14 GPa [15,16]. In the decompressed Raman data, additional peaks are seen at 850 and 1300 cm^{-1}. These peaks may occur either due to the increased disorder in the sp^3 system or the signals from the phase transformed grain boundary carbon network [45], and more experiments are being carried out to confirm this. The dp^3-bonded phase remains intact, as shown by the 500 and 1200 cm^{-1} bands in the decompressed Raman spectrum, and we will further validate this by using a pressure-dependent XRD measurement. Since all the Raman modes in BDD undergo a blueshift, it is likely that these modes are stretching modes.

C. High-pressure XRD

On the other hand, properties of the bulk modulus B_0 and its pressure derivative $B_0' = \frac{dB_0}{dP}$ give valuable insight into the bonding nature of solids. It is well reported that the cubic diamond phase remains stable up to 140 GPa and its $B_0 = 442$ GPa [14] and $B_0' = 3.6$ are well known. However, similar information for superconducting CVD-grown BDD is still missing and needs to be investigated. As the observed changes in the pressure coefficient occur in the Raman modes originating from the sp^3 grains, it is tempting to attribute this observation to a phase change in the sp^3-bonded grains. The pressure-dependent XRD results in Figs. 3(a) and 3(b) suggest otherwise. High-pressure XRD results show that the cubic phase of superconducting BDD remains intact up to 30 GPa. Hence, it is unlikely that the abrupt change in the pressure coefficient is due to a phase change in the sp^3-bonded carbon atoms. A plausible explanation for this may be that the doubling of the pressure coefficient is driven by the phase transformation in the grain boundaries. We believe that the pressure coefficient doubling above 14 GPa in the superconducting BDD is due to the conversion of an sp^2 to sp^3 phase in the grain boundaries. Surprisingly, this new phase of sp^3-hybridized atoms leads to an increase in the pressure coefficient, defying conventional wisdom that an increase in the coordination number decreases the pressure coefficient [46,47]. One plausible explanation for this is that the newly formed sp^3 phase above 14 GPa has larger atom-atom bond lengths [48] than cubic diamond, thereby influencing the ease of compression (or increasing the pressure coefficient) of the whole system. Figure 3(b) shows the least square fittings of our $P-V$ data using Vinet's equations of state (EOS) [49], which gives $V_0 = 45.70$ $Å^3$, $B_0 = 510$ GPa, and $B_0' = 2.6$. The error bars indicate standard deviations in the estimation of the unit cell volume using the lattice parameters a_{111},

TABLE I. Summary of the pressure coefficient (cm^{-1} GPa^{-1}) of various Raman modes in granular BDD. We show the pressure coefficient ($\frac{dw_i}{dp}$) at pressures <14 and at >14 GPa.

Vibrational modes	B-B mode	1000 cm^{-1}	1200 cm^{-1}	D peak	ν_3
$\frac{dw_i}{dp}$ (<14 GPa)	6.3	0.8	3.24	7.1	7.1
$\frac{dw_i}{dp}$ (>14 GPa)	11.9	1.6	Masked by anvil	Phase change	Phase change

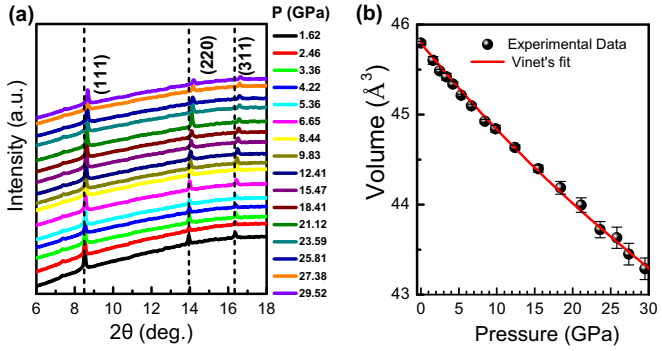

FIG. 3. (a) Representative XRD patterns of BDD under various pressures. The dotted lines indicate the shift of the diffraction peaks, a result of lattice contraction under compression. The extra peak at 7.32° is due the Fe in the steel gasket. (b) Volume change vs the applied pressure behavior of BDD, where the solid spheres represent the volume at a given pressure and the continuous curve represents a fit to the Vinet's equation.

a_{220}, and a_{311}. Unit cell deformation because of random boron incorporation is obvious. However, this deformation becomes noticeably large at higher pressures, as indicated by the error bars. The impressively large B_0 in our CVD-grown superconducting BDD thick film is noteworthy, and although this value is smaller than the optical grade polycrystalline diamond films [50], it is certainly larger than HPHT-grown BDD [51,52] or cubic BC_5 [53]. B_0 depends significantly on the grain sizes [54,55]. It is also possible that the presence of an isolated boron-rich secondary phase in the sp^3-bonded grains [7,18] may influence the value of B_0 in HPHT-grown BDD.

Finally, we discuss the relevance of phonon-mediated mechanisms in the grains by conducting high-pressure transport studies. In Fig. 4, we show our pressure-dependent

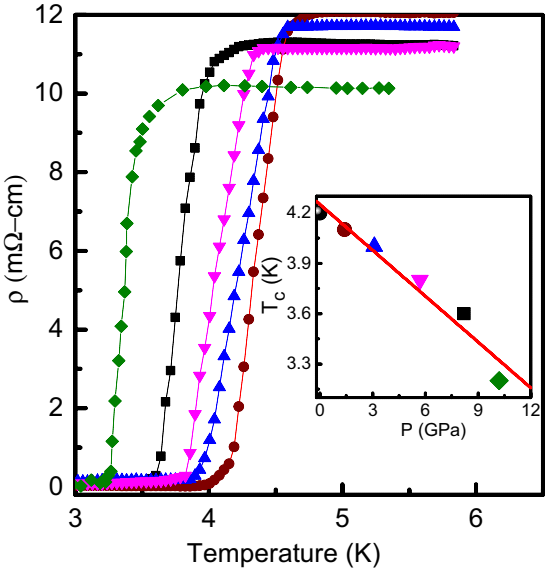

FIG. 4. Temperature dependence of resistivity under various applied pressures. Superconductivity is suppressed with increasing pressure. Inset: Pressure-induced suppression of the T_c.

resistivity curves. In our experiment, T_c reduces with applied pressure by a pressure coefficient of −0.09 K/GPa, which is slightly larger than the pressure coefficient of −0.06 K/GPa, reported by Ekimov *et al.* [2]. The suppression of superconductivity at high pressure via a decrease of the electron-phonon coupling parameter in BDD has been theoretically demonstrated [56]. Ma *et al.* pointed out that the decrease in the electronic density of states (N) near the Fermi level and the weakening of $\lambda_{\text{el-ph}}$ with an increase in pressure causes T_c depression [56]. From our result and also in the publication by Tomioka *et al.* [57], a decrease in ρ_n is observed with an increase in pressure. This undermines the possibility of the reduction of N with an increase in pressure. Thus, hardening of the Raman ZCP mode, which is well known in the case of intrinsic diamond [14,58], however, unfortunately masked by the signals from the DAC in the present experiment, is the most likely reason for the T_c depression under pressure. This has important implications for coupling between the phonon and holes. In the BCS formulation, $\lambda_{\text{el-ph}} = \frac{ND}{M\omega^2}$, where D is the deformation potential and M is the mass of the C atom. However, $\lambda_{\text{el-ph}}$ is related to T_c as $T_c \propto \exp(-\frac{1}{\lambda_{\text{el-ph}}})$. Therefore, a decrease in $\lambda_{\text{el-ph}}$ with pressure results in the reduction of T_c. Hence, T_c suppression with applied pressure can be attributed to the hardening of the Raman mode.

IV. CONCLUSIONS

In summary, we used the CVD method, one of the most promising ways to grow BDD, to investigate the details of its bonding, vibrational properties, and possible phase changes at high pressures. The grain boundary components undergo an irreversible phase change at 14 GPa. The pressure coefficient values increased from 6.3 and 0.8 cm^{-1}/GPa to 11.9 and 1.6 cm^{-1}/GPa, for the Raman modes at 455 and 1000 cm^{-1}, respectively. We found a high bulk modulus, $B_0 = 510$ GPa, in our CVD-grown BDD thick film. We show that the blueshift in the pressure-dependent vibrational modes correlates with the negative pressure coefficient of T_c in BDD. By comparing our high-pressure XRD and Raman scattering results, we show that the sp^2 carbons in the grain boundaries transform into hexagonal diamond.

ACKNOWLEDGMENTS

We are grateful to Goran Karapetrov, Jiuhau Chen, Jun Zhao, and Donglai Feng for stimulating discussions. The work in Russia was supported in part from the Ministry of Education and Science of the Russian Federation in the framework of Increase Competitiveness Program of NUST "MISiS" (K2-2016-066) and by Act 211 of the Russian Federation Government, Contracts No. 02.A03.21.0006 and No. 02.A03.21.0011. D.K. and M.S.R.R. would like to thank the financial support from Department of Science and Technology (DST), New Delhi, that led to the establishment of Nano Functional Materials Technology Centre (NFMTC) (SR/NM/NAT/02-2005) and the Department of Atomic Energy (DAE).

[1] X. Blase, E. Bustarret, C. Chapelier, T. Klein, and M. Christophe, Nat. Mater. **8**, 375 (2009).
[2] E. Ekimov, V. Sidorov, E. Bauer, N. Mel'Nik, N. Curro, J. Thompson, and S. Stishov, Nature (London) **428**, 542 (2004).
[3] H. Okazaki *et al.*, Appl. Phys. Lett. **106**, 052601 (2015).
[4] J. E. Moussa and M. L. Cohen, Phys. Rev. B **77**, 064518 (2008).
[5] J. Goss and P. Briddon, Phys. Rev. B **73**, 085204 (2006).
[6] Y. H. Chen, C. T. Hu, and I. N. Lin, Appl. Phys. Lett. **75**, 2857 (1999).
[7] N. Dubrovinskaia, R. Wirth, J. Wosnitza, T. Papageorgiou, H. F. Braun, N. Miyajima, and L. Dubrovinsky, Proc. Natl. Acad. Sci. USA **105**, 11619 (2008).
[8] J. J. Mareš, M. Nesladek, P. Hubík, D. Kindl, and J. Krištofik, Diamond Relat. Mater. **16**, 1 (2007).
[9] L. Boeri, J. Kortus, and O. K. Andersen, Phys. Rev. Lett. **93**, 237002 (2004).
[10] X. Blase, C. Adessi, and D. Connetable, Phys. Rev. Lett. **93**, 237004 (2004).
[11] G. Baskaran, J. Supercond. Novel Magn. **21**, 45 (2008).
[12] T. Klein, P. Achatz, J. Kacmarcik, C. Marcenat, F. Gustafsson, J. Marcus, E. Bustarret, J. Pernot, F. Omnes, B. E. Sernelius *et al.*, Phys. Rev. B **75**, 165313 (2007).
[13] G. Baskaran, Sci. Tech. Adv. Mater **7**, S49 (2006).
[14] F. Occelli, P. Loubeyre, and R. LeToullec, Nat. Mater. **2**, 151 (2003).
[15] M. Hanfland, H. Beister, and K. Syassen, Phys. Rev. B **39**, 12598 (1989).
[16] A. Brillante, M. Hanfland, K. Syassen, and J. Hocker, Physica C **139**, 533 (1986).
[17] M. Salehpour and S. Satpathy, Phys. Rev. B **41**, 3048 (1990).
[18] Y. Lu, S. Turner, E. A. Ekimov, J. Verbeeck, and G. Van Tendeloo, Carbon **86**, 156 (2015).
[19] S. Turner, Y. Lu, S. D. Janssens, D. P. Fabiana, D. Lamoen, J. Verbeeck, K. Haenen, P. Wagner, and V. G. Tendeloo, Nanoscale **4**, 5960 (2012).
[20] Y. Lu, S. Turner, J. Verbeeck, S. D. Janssens, K. Haenen, and G. V. Tendeloo, Appl. Phys. Lett. **103**, 032105 (2015).
[21] Y. Lu, S. Turner, J. Verbeeck, S. D. Janssens, P. Wagner, K. Haenen, and G. V. Tendeloo, Appl. Phys. Lett. **101**, 041907 (2012).
[22] G. Zhang, S. Turner, E. A. Ekimov, J. Vanacken, M. Timmermans, T. Samuely, V. A. Sidorov, S. M. Stishov, Y. Lu, B. Deloof *et al.*, Adv. Mater. **26**, 2034 (2014).
[23] V. Mortet, Z. V. Živcová, A. Taylor, O. Frank, P. Hubík, D. Trémouilles, F. Jomard, J. Barjon, and L. Kavan, Carbon **115**, 279 (2017).
[24] M. Chandran, B. Tiwari, C. R. Kumaran, S. K. Sunil, S. S. Bhattacharya, and M. S. R. Rao, J. Phys. D: Appl. Phys. **45**, 202001 (2012).
[25] M. Abdel-Hafiez, X.-M. Zhao, A. A. Kordyuk, Y.-W. Fang, B. Pan, Z. He, C.-G. Duan, J. Zhao, and X.-J. Chen, Sci. Rep. **6**, 31824 (2016).
[26] E. Bustarret, J. Kačmarčik, C. Marcenat, E. Gheeraert, C. Cytermann, J. Marcus, and T. Klein, Phys. Rev. Lett. **93**, 237005 (2004).
[27] N. R. Werthamer, E. Helfand, and P. C. Hohenberg, Phys. Rev. **147**, 295 (1966).
[28] A. M. Clogston, Phys. Rev. Lett. **9**, 266 (1962).
[29] B. Chandrasekhar, Appl. Phys. Lett. **1**, 7 (1962).
[30] M. Bernard, A. Deneuville, and P. Muret, Diamond Relat. Mater. **13**, 282 (2004).
[31] S. Prawer and R. J. Nemanich, Philos. Trans. R. Soc. A **362**, 1824 (2004).
[32] P. W. May, W. J. Ludlow, M. Hannaway, P. J. Heard, J. A. Smith, and K. N. Rosser, Diamond Relat. Mater. **17**, 105 (2008).
[33] S. Johnston, M. Abdel-Hafiez, L. Harnagea, V. Grinenko, D. Bombor, Y. Krupskaya, C. Hess, S. Wurmehl, A. U. B. Wolter, B. Büchner, H. Rosner, and S.-L. Drechsler, Phys. Rev. B **89**, 134507 (2014).
[34] M. Abdel-Hafiez, S. Aswartham, S. Wurmehl, V. Grinenko, C. Hess, S.-L. Drechsler, S. Johnston, A. U. B. Wolter, B. Büchner, H. Rosner, and L. Boeri, Phys. Rev. B **85**, 134533 (2012).
[35] M. Abdel-Hafiez, P. J. Pereira, S. A. Kuzmichev, T. E. Kuzmicheva, V. M. Pudalov, L. Harnagea, A. A. Kordyuk, A. V. Silhanek, V. V. Moshchalkov, B. Shen, H.-H. Wen, A. N. Vasiliev, and X.-J. Chen, Phys. Rev. B **90**, 054524 (2014).
[36] M. Abdel-Hafiez, Y.-Y. Zhang, Z.-Y. Cao, C.-G. Duan, G. Karapetrov, V. M. Pudalov, V. A. Vlasenko, A. V. Sadakov, D. A. Knyazev, T. A. Romanova, D. A. Chareev, O. S. Volkova, A. N. Vasiliev, and X.-J. Chen, Phys. Rev. B **91**, 165109 (2015).
[37] V. Sidorov, E. Ekimov, S. Stishov, E. Bauer, and J. Thompson, Phys. Rev. B **71**, 060502 (2005).
[38] B. L. Willems, V. H. Dao, J. Vanacken, L. F. Chibotaru, V. V. Moshchalkov, I. Guillamón, H. Suderow, S. Vieira, S. D. Janssens, O. A. Williams *et al.*, Phys. Rev. B **80**, 224518 (2009).
[39] A. C. Victor, J. Chem. Phys. **36**, 1903 (1962).
[40] P. Szirmai, T. Pichler, O. A. Williams, S. Mandal, C. Bäuerle, and F. Simon, Phys. Status Solidi B **249**, 2656 (2012).
[41] E. Bourgeois, E. Bustarret, P. Achatz, F. Omnès, and X. Blase, Phys. Rev. B **74**, 094509 (2006).
[42] A. Ferrari and J. Robertson, Phys. Rev. B **63**, 121405 (2001).
[43] P. V. Zinin, L. C. Ming, I. Kudryashov, N. Konishi, M. H. Manghnani, and S. K. Sharma, J. Appl. Phys. **100**, 013516 (2006).
[44] B. A. Weinstein and R. Zallen, *Light Scattering in Solids IV* (Springer, Berlin, 1984), pp. 463–527.
[45] D. S. Knight and W. B. William, J. Mater. Res. **4**, 385 (1989).
[46] W. F. Sherman, J. Phys. C **13**, 4601 (1980).
[47] R. Zallen, Phys. Rev. B **9**, 4485 (1974).
[48] T. Yagi, W. Utsumi, M. Yamakata, T. Kikegawa, and O. Shimomura, Phys. Rev. B **46**, 6031 (1992).
[49] P. Vinet, J. R. Smith, J. Ferrante, and J. H. Rose, Phys. Rev. B **35**, 1945 (1987).
[50] K. J. Gray, Proc. SPIE **1759**, 203 (1992).
[51] E. Ekimov, V. Ralchenko, and A. Popovich, Diamond Relat. Mater. **50**, 15 (2014).
[52] N. Dubrovinskaia, L. Dubrovinsky, W. A. Crichton, E. Zarechnaya, E. I. Isaev, and I. A. Abrikosov, High Press. Res. **26**, 79 (2006).
[53] V. L. Solozhenko, O. O. Kurakevych, D. Andrault, Y. L. Godec, and M. Mezouar, Phys. Rev. Lett. **102**, 015506 (2009).
[54] N. Dubrovinskaia, L. Dubrovinsky, W. Crichton, F. Langenhorst, and A. Richter, Appl. Phys. Lett. **87**, 083106 (2005).

[55] O. A. Williams, A. Kriele, J. Hees, M. Wolfer, W. Müller-Sebert, and C. E. Nebel, Chem. Phys. Lett. **495**, 84 (2010).

[56] Y. Ma, S. T. John, T. Cui, D. D. Klug, L. Zhang, Y. Xie, Y. Niu, and G. Zou, Phys. Rev. B **72**, 014306 (2005).

[57] F. Tomioka, S. Tsuda, T. Yamaguchi, H. Kawarada, and Y. Takano, Phys. C **468**, 1228 (2008).

[58] M. Hanfland, K. Syassen, S. Fahy, S. G. Louie, and M. L. Cohen, Phys. Rev. B **31**, 6896 (1985).